BIOLOGY OF REPRODUCTION **77,** 551–559 (2007)
Published online before print 6 June 2007.
DOI 10.1095/biolreprod.107.061358

CATSPER Channel-Mediated Ca^{2+} Entry into Mouse Sperm Triggers a Tail-to-Head Propagation[1]

Jingsheng Xia,[3] David Reigada,[4] Claire H. Mitchell,[4] and Dejian Ren[2,3]

Department of Biology[3] and Department of Physiology,[4] University of Pennsylvania, Philadelphia, Pennsylvania 19104

ABSTRACT

Many Ca^{2+} channel proteins have been detected in mammalian sperm, but only the four CATSPER channels have been clearly shown to be required for male fertility. Ca^{2+} entry through the principal piece-localized CATSPER channels has been implicated in the activation of hyperactivated motility. In the present study, we show that the Ca^{2+} entry also triggers a tail-to-head Ca^{2+} propagation in the mouse sperm. When activated with 8-Br-cAMP, 8-Br-cGMP, or alkaline depolarization, a CATSPER-dependent increase in intracellular Ca^{2+} concentration starts in the principal piece, propagates through the midpiece, and reaches the head in a few seconds. The Ca^{2+} propagation through the midpiece leads to a Ca^{2+}-dependent increase in NADH fluorescence. In addition, *CatSper1*-mutant sperm have lower intracellular ATP levels than wild-type sperm. Thus, a Ca^{2+} influx in the principal piece through CATSPER channels can not only initiate hyperactivated motility, but can also trigger a tail-to-head Ca^{2+} propagation that leads to an increase in [NADH] and may regulate ATP homeostasis.

acrosome reaction, calcium, sperm capacitation, sperm motility and transport

INTRODUCTION

During mammalian fertilization, Ca^{2+} signaling plays a central role in essentially every step, from sperm capacitation and motility to the fusion between sperm and egg [1]. The cytosolic Ca^{2+} concentration ($[Ca^{2+}]_i$) can be raised by either Ca^{2+} influx through plasma membrane ion channels or Ca^{2+} release from intracellular stores. The low $[Ca^{2+}]_i$ is maintained through mechanisms involving the plasma membrane Ca^{2+} pump ATPase and mitochondria [2]. Increases in $[Ca^{2+}]_i$ can induce the exocytotic acrosome reaction (AR) in the head and trigger sperm hyperactivation in the tail [3, 4].

Several Ca^{2+}-permeable ion channel proteins have been found in mammalian sperm. They include voltage-gated Ca^{2+} channels, transient receptor potential (TRP) channels, cyclic nucleotide-gated channels, and CATSPER channels [5, 6]. However, only the four mammalian *CatSper* members (*CatSpers* 1–4) are restrictively expressed in the testis and are clearly shown to be required for male fertility [7–11]. The four CATSPER proteins are primarily localized to the plasma membrane of the distal portion of the sperm tail, the principal piece, and presumably form a heterotetrameric, pH- and voltage-dependent Ca^{2+}-permeable channel [7, 8, 11, 12]. Male mice deficient in any of the four CATSPERs are completely sterile but exhibit no other apparent abnormality. The major phenotypes of the null sperm are a lack of hyperactivated motility, a gradual loss of motility after isolation, and an inability to penetrate zona-intact eggs [8, 11, 13, 14].

Cyclic GMP and cAMP are each able to cause $[Ca^{2+}]_i$ increases in both the head and tail [8, 15, 16]. Intriguingly, both of the $[Ca^{2+}]_i$ increases are abolished by a targeted disruption in the CATSPER1 channel [8, 12, 14, 17]. In this report, we show that Ca^{2+} influx, induced by either cell-permeable cyclic nucleotides or alkaline depolarization, initiates a Ca^{2+} propagation that starts in the principal piece and arrives at the head in several seconds. The CATSPER-dependent $[Ca^{2+}]_i$ increases apparently are not involved in the AR. Instead, the Ca^{2+} signal leads to an increase in the NADH level in the sperm midpiece. Furthermore, *CatSper1*-mutant sperm have a decreased intracellular ATP level compared with the wild-type (WT) sperm. Thus, Ca^{2+} influx from CATSPER channels not only affects sperm hyperactivated motility but also may regulate ATP homeostasis.

MATERIALS AND METHODS

Reagents

Reagents were from Sigma unless otherwise stated. Fluo-4 AM and pluronic F-127 were from Molecular Probes (Invitrogen, Eugene, OR). Cell-Tak was from BD Biosciences (Bedford, MA). Coomassie Blue G-250 and mounting medium (Permount) were from Fisher Scientific (Pittsburg, PA). Paraformaldehyde was from Electron Microscopy Services (Hatfield, PA).

Cell Preparation

Animal uses followed guidelines approved by IACUC (Institutional Animal Care and Use Committee) at the University of Pennsylvania. The *CatSper1*-mutant strain had been backcrossed to C57BL/6 for more than 10 generations [8]. The GFP-CATSPER1 transgenic mice carried a transgene encoding GFP and CATSPER1 (GFP at the amino-terminus; driven by a *CatSper1* promoter) in the *CatSper1*-null background. The transgene fully rescued the male sterile phenotype of the *CatSper1* null. Details of the generation of these mice will be described elsewhere. Experiments involving mutant/WT paired preparations were done in a blind manner in which the experimentalist did not know the genotype until after initial data analysis. Age-paired mice, from 3 to 6 mo old, were used for sperm collection. Mice were killed with CO_2 asphyxiation, followed by cervical dislocation. Caudal epididymides were excised and rinsed with HS medium [18] containing (millimolar) 135 NaCl, 5 KCl, 2 $CaCl_2$, 1 $MgCl_2$, 30 Hepes, 10 glucose, 10 lactic acid, and 1 pyruvic acid (pH adjusted to 7.4 with NaOH). Caudal sperm were released from three small incisions at 37°C in a 5% CO_2 incubator for 15 min into HS medium supplemented with 4 mg/ml BSA and 15 mM $NaHCO_3$. Sperm were concentrated to 5×10^6 to 1×10^7/ml by centrifugation for 5 min at $400 \times g$. For ATP measurement and Ca^{2+} imaging with cyclic nucleotides and K8.6, sperm were used without capacitation.

Ca^{2+} Imaging

Cells were loaded with 10 μM Fluo-4 AM and 0.05% pluronic F-127 for 30 min at room temperature in the dark and then washed twice in HS medium,

[1]Supported by NIH grants 1R01HD047578, 1R03HD045290, and 1R01EY013434 and the University of Pennsylvania Research Foundation.
[2]Correspondence: Dejian Ren, Department of Biology, University of Pennsylvania, 415 South University Ave., Philadelphia, PA 19104. FAX: 215 898 8780; e-mail: dren@sas.upenn.edu

Received: 8 March 2007.
First decision: 4 April 2007.
Accepted: 30 May 2007.

ISSN: 0006-3363. http://www.biolreprod.org

each with a 5-min spin at 400 × *g*. Washed sperm were resuspended in HS medium, plated onto coverslips coated with Cell-Tak, and allowed to attach for ~10 min. Small volume imaging chambers (~1 cm in diameter, ~90 μl) were formed with Sylgard on coverslips. A monochromator (DeltaRAM V; PTI, Birmingham, NJ) with a 75-W Xenon lamp was used to generate excitation at 488 nm. A 60× PlanApo water immersion objective (numerical aperture 1.2; Olympus) and a 1.6× adaptor (total magnification of 96×) on an inverted microscope (IX-71; Olympus) were used for imaging. Emissions between 515 and 565 nm were filtered through a band-pass filter (HQ540/50; Chroma, Rockingham, VT). Signals were collected through a cooled, charge-coupled device camera (CoolSNAP HQ; Roper Scientific, Trenton, NJ) for 25 msec every 500 msec. Online control, data collection, and image analysis were done by commercial software (ImageMaster 3; PTI). $[Ca^{2+}]_i$ changes were represented as $\Delta F{:}F_0$ ratios after background subtraction, where ΔF was the change in fluorescence signal intensity, and F_0 was the baseline calculated as the average of the seven frames prior to stimulus application. All Ca^{2+} imaging experiments were done at room temperature (~22 to 25°C). Cells with uneven dye loading were excluded from analysis. Only moderately motile sperm (identified by comparing multiple image frames) that had one or two points attached to the coverslip were used for analysis. The cell-permeable cGMP (8-Br-cGMP) and cAMP (8-Br-cAMP) (resuspended in H_2O) were used at 2 and 1 mM, respectively, similar to the 0.3–3 mM range used by other researchers [16]. These concentrations gave robust Ca^{2+} responses in the WT sperm [16] (see Supplemental Fig. S1). The alkaline high potassium solution (K8.6) used in Ca^{2+} imaging contained (millimolar) 135 KCl, 5 NaCl, 2 $CaCl_2$, 1 $MgCl_2$, 10 glucose, 10 lactic acid, 1 pyruvic acid, and 30 TAPS (*N*-Tris(hydroxymethyl)-methyl-3-aminopropanesulfonic acid, with pH adjusted to 8.6 with NaOH) [18]. Stimuli were applied by dropping into the bath with pipette tips (in 10 μl) or by perfusion (for K8.6; ~1 ml at 3 ml/min), and recordings were done in the continuous presence of the stimuli.

Detection of Capacitation and AR with the Chlortetracycline Fluorescence Assay

The chlortetracycline (CTC) assay was performed as described previously [19, 20]. Sperm suspensions (5×10^6 to 5×10^7/ml) were incubated for 75 min at 37°C, 5% CO_2, in a modified HMB capacitation medium containing (millimolar): 109 NaCl, 4.77 KCl, 1.71 $CaCl_2$, 1.19 $MgSO_4$, 1.19 KH_2PO_4, 5.56 glucose, 25 sodium lactate, 1 sodium pyruvate, 25 $NaHCO_3$, BSA (4 mg/ml), and 25 Hepes (pH adjusted to 7.3 with NaOH) [21]. Aliquots (100 μl) of capacitated sperm were treated for 15 min with one of the following AR inducers: 5 μM ionomycin, 10 μM A23187, 2 mM 8-Br-cGMP, or a modified K8.6 containing (millimolar) 60 KCl, 54 NaCl, 2 $CaCl_2$, 1 $MgCl_2$, 10 glucose, 10 lactic acid, 1 pyruvic acid, and 30 TAPS (pH adjusted to 8.6 with NaOH) [22]. Like the K8.6 medium used for Ca^{2+} imaging, the modified K8.6 also induced robust $[Ca^{2+}]_i$ rises in sperm (see Supplemental Fig. S2). Non-capacitated sperm and capacitated but nontreated sperm were used as negative controls. Fifty microliters of each reaction was mixed for several seconds with equal amounts of prewarmed CTC solution (millimolar: 0.5 CTC, 130 NaCl, 5 cysteine, and 20 Tris-HCl, pH 7.8), followed by fixation with 8 μl of 12.5% (w/v) paraformaldehyde in PBS [20]. About 10 μl of each suspension was applied onto coverslips and examined for CTC fluorescence with a 60× objective on an inverted microscope (excitation at 400 nm and emission at 515–565 nm). Three separate experiments were performed for each treatment. At least 100 sperm cells on each slide were examined and assigned to one of the following three staining patterns: noncapacitated (pattern "F"), capacitated but not acrosome reacted (pattern "B"), and acrosome reacted (pattern "AR") [19, 20].

Detection of the AR with Coomassie Blue Staining

AR detection with Coomassie Blue G-250 was performed by a slight modification of previously described methods [23–25]. Capacitated sperm treated with AR inducers were washed and fixed with 4% paraformaldehyde solution (110 mM Na_2HPO_4, 2.5 mM NaH_2PO_4, and 4% paraformaldehyde, pH 7.4 adjusted with NaOH) for 10 min at room temperature. Fixed sperm were washed twice in ammonium acetate (100 mM, pH 9.0) and resuspended in the same solution. Fifteen microliters of the sperm suspension was smeared onto a glass slide, air dried, and incubated for 2 min in freshly prepared Coomassie staining solution containing 0.22% Coomassie Blue G-250, 50% methanol, and 10% Glacial acetic acid. The slides were washed thoroughly with water to remove excess stain. Coverslips were then mounted onto the air-dried slides with mounting medium (Permount) and sealed with nail oil. Stained sperm were examined under the microscope at 600×. A minimum of 10 fields (>100 sperm each) per slide and three separate experiments for each treatment were examined.

NADH Autofluorescence Imaging

NADH imaging experiments were done at 37°C with a heated stage. Capacitated sperm were washed, resuspended in imaging buffer (HS medium supplemented with 15 mM $NaHCO_3$), and plated onto coverslips coated with Cell-Tak. NADH fluorescence was excited with UV light from 354 to 366 nm, and emission was collected with a 435–485 band-pass filter (set 3100V2; Chroma) [26–28]. To ensure that only preparations with stable baselines were included, imaging buffer was applied as a test before other stimuli. Sampling frequency was one frame each 12 sec, and sampling duration was 300 msec. Signals from the midpiece were averaged, background subtracted, and normalized to the baseline (F_0, calculated as the average of 10 frames before stimulus application).

ATP Measurement

Sperm suspensions of 0.4 ml (5×10^5 to 1.8×10^6 sperm/ml) were treated with HS buffer or HS containing 2 mM 8-Br-cGMP for 3 min. ATP was extracted by boiling for 10 min [29]. After cooling down on ice, the suspensions were centrifuged for 5 min at 500 × *g* (4°C), and the supernatants were collected. ATP levels were measured in triplicate or quadruplicate samples on 96-well plates with the luciferase-based ATP bioluminescent assay kit (Sigma) with a luminometer (Luminoskan Ascent; Thermo Labsystems, Franklin, MA) as previously described [30]. After injecting 10 μl of luciferase-containing solution (in HS) to a 90-μl sample in a well, readings were integrated over 100 msec and sampled every 30 sec for 5 min (total of 10 readings per sample). Standard curves were constructed from measurements with boiled HS solutions containing ATP (for HS treatment) or HS solutions containing ATP and 2 mM 8-Br-cGMP (for 8-Br-cGMP treatment).

Data Analysis

Data analyses were performed by Excel and Origin. Data are presented as mean ± SEM. Two-tailed Student *t*-tests was used to calculate statistical significance.

RESULTS

A CATSPER-Dependent, Tail-to-Head Ca^{2+} Propagation in Mouse Sperm Induced by Cell-Permeable cGMP and cAMP

By single-cell Ca^{2+} imaging analysis, we and other researchers previously observed that 8-Br-cAMP and 8-Br-cGMP induced increases in $[Ca^{2+}]_i$ in both sperm head and tail [8, 15, 16]. The image sampling frequency in our previous studies (0.2 Hz) did not allow detailed analysis of kinetics differences in sperm subregions. We could not determine whether the $[Ca^{2+}]_i$ increases in the different cellular domains were independent of each other (e.g., through different Ca^{2+} influx pathways) or were the consequence of Ca^{2+} propagation. In this study, we have adapted a system that allowed us to image at 2 Hz (0.5 sec/frame). When 8-Br-cGMP (2 mM) was applied to the bath with sperm loosely attached to the coverslips, increases in $[Ca^{2+}]_i$, as indicated by fluorescence changes normalized to the baseline, were observed in the majority (>90%) of cells. The increases clearly started from the principal piece, followed by increases in the midpiece and the head (Fig. 1, A and C). The changes in the tail were transient, even in the continuous presence of 8-Br-cGMP. The increases in the head, however, were more sustained (Fig. 1A).

By measuring the time differences between the application of 8-Br-cGMP and the onset of fluorescence increase in each region, we found a delay of 3.2 ± 0.2 sec (n = 21) between the head and principal piece in the $[Ca^{2+}]_i$ changes (Fig. 1C). There was also a delay (1.0 ± 0.2 sec) between two points ~5 μm apart within the midpiece (MP1 and MP2 in Fig. 1C). In contrast, no significant delay (0.15 ± 0.16 sec) was observed between two points of similar distance within the principal piece (PP1 and PP2 in Fig. 1C). When Ca^{2+} ionophore ionomycin (5 μM) was used to stimulate $[Ca^{2+}]_i$ increases, no

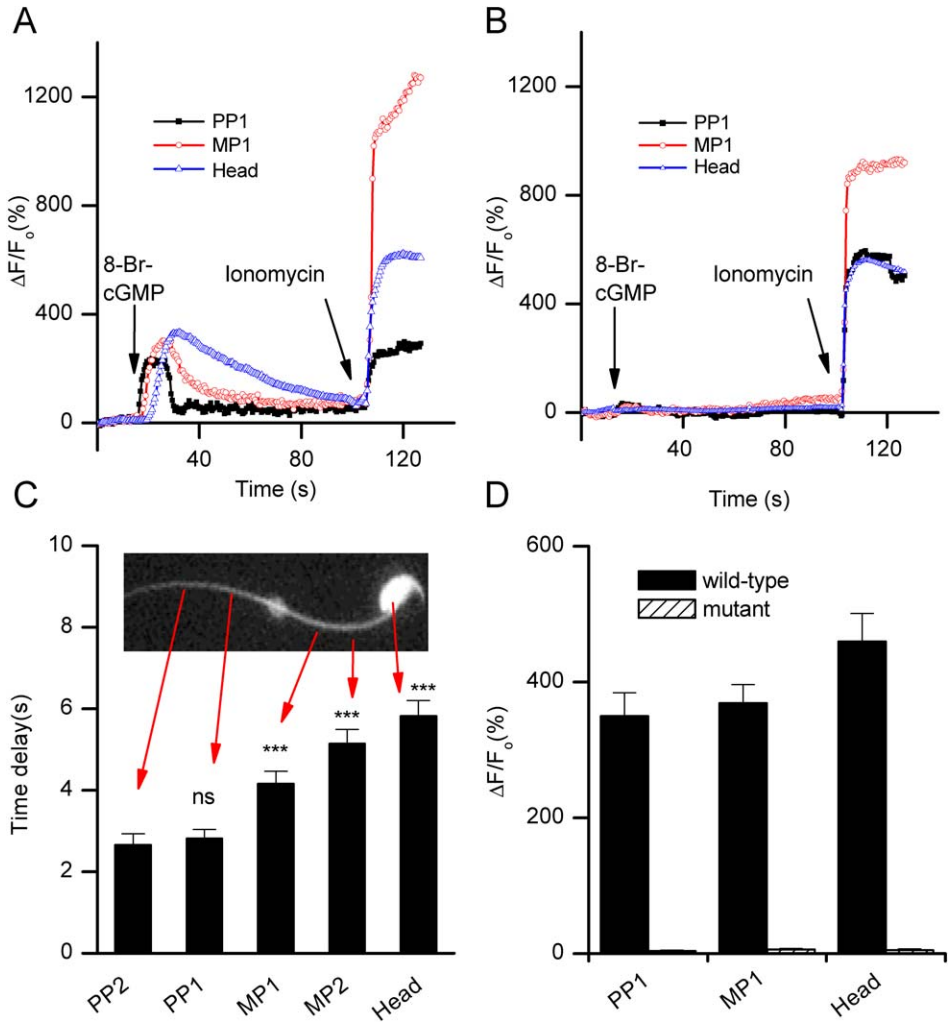

FIG. 1. A CATSPER-dependent, tail-to-head Ca^{2+} propagation induced by 8-Br-cGMP in mouse sperm. Representative time courses of the $[Ca^{2+}]_i$ change (represented as the Fluo-4 fluorescence changes) in the principal piece (PP1), midpiece (MP1), and head from a WT (**A**) and *CatSper1*-mutant (**B**) sperm are shown. The fluorescence changes were abolished in the three regions in the mutant sperm, as also shown in the averaged peak responses (**D**, n = 27 for WT and 11 for mutant). In the WT, increases in $[Ca^{2+}]_i$ started in the principal piece and propagated to the head, as reflected by the time differences between the application of 8-Br-cGMP and the onset of fluorescence change (defined as the time point when $\Delta F/F_0$ started to have a steep rise) (**C**, n = 21). Ca^{2+} ionophore ionomycin (5 μM) induced $[Ca^{2+}]_i$ rises simultaneously in all the subregions (**A**, **B**). Arrows indicate time points when the stimuli were applied. The locations of the subregions within the principal piece (PP1 and PP2), midpiece (MP1 and MP2), and head chosen for analysis are indicated in the inset (**C**). PP1 and MP1 are both ~5 μm from the annulus. There is a ~5-μm distance from PP1 to PP2 and from MP1 to MP2. CATSPER1 protein is localized to the principal piece [8]. See also the movie in Supplemental Material showing the wavelike propagation of $[Ca^{2+}]$ increases along the sperm after the application of 8-Br-cGMP. In Figs. 1–3, ns indicates not statistically significant compared with PP2 ($P > 0.05$); *, statistically significant ($P < 0.05$); ***, statistically significant ($P < 0.001$).

delay was observed between any of the regions along the whole sperm (Fig. 1A). Consistent with previous findings [8], no significant $[Ca^{2+}]$ increase was detected in any of the regions in the *CatSper1*-mutant sperm (Fig. 1, B and D). These data suggest that the 8-Br-cGMP-induced increase in $[Ca^{2+}]_i$ starts simultaneously within the principal piece but gradually propagates toward the head (Fig. 2 and Supplemental Movie, available at www.biolreprod.org). The simultaneous $[Ca^{2+}]_i$ increases along the principal piece, and the restricted localization of CATSPER1 protein to the same region [8], are consistent with the hypothesis that the 8-Br-cGMP-induced Ca^{2+} entry through CATSPER channels serves as a trigger for a tail-to-head Ca^{2+} propagation.

Similar to 8-Br-cGMP, 8-Br-cAMP caused $[Ca^{2+}]_i$ increases in sperm tail and head (Fig. 3A). There was a delay of 3.7 ± 0.4 sec between the onsets of $[Ca^{2+}]_i$ increases in the head and the principal piece, but no significant delay was detected between two subregions within the principal piece (Fig. 3B).

Tail-to-Head Ca^{2+} Propagation Induced by Alkaline Depolarization

The 8-Br-cGMP- and 8-Br-cAMP-induced tail-to-head Ca^{2+} propagation described above is reminiscent of a similar $[Ca^{2+}]$ change in the sea urchin sperm challenged with speract, an egg peptide that induces [cGMP] changes in sperm [31]. We wondered if the tail-to-head Ca^{2+} propagation was a unique feature of cyclic nucleotides-induced Ca^{2+} signaling. Depolarization, when coupled with alkalization (K8.6), was shown to elicit a CATSPER-dependent $[Ca^{2+}]_i$ increase in mouse sperm [14, 18, 32], but the spatial-temporal kinetics of the $[Ca^{2+}]$ changes were not resolved in the previous studies. When sperm were exposed to the continuous presence of K8.6, $[Ca^{2+}]_i$ increases were observed in both heads and tails (Fig. 4, A and D). Like the 8-Br-cGMP-induced increases in $[Ca^{2+}]_i$, the K8.6-induced increases started from the tail and spread to the head with a delay of ~6 sec (Fig. 4, A and C). No time delay was observed within the principal piece. Consistent with previous studies [14], no significant $[Ca^{2+}]_i$ increase was observed in any of the regions in the CATSPER1-deficient sperm (Fig. 4, B and D). The increases in $[Ca^{2+}]_i$ induced by the continuous presence of K8.6 were more sustained in all the three segments than those induced by 8-Br-cGMP. These observations suggest that both K8.6 and cyclic nucleotides are able to induce a tail-to-head Ca^{2+} propagation triggered by Ca^{2+} entry through CATSPER channels.

The CATSPER-Mediated $[Ca^{2+}]_i$ Increases Are Not Required for the AR

$[Ca^{2+}]_i$ increases are often associated with sperm capacitation, a process by which sperm become competent to fertilize the eggs, and the AR, a Ca^{2+}-dependent exocytotic process by which sperm release the acidic acrosomal contents [1, 3]. Because the CATSPER-mediated Ca^{2+} entry triggers a tail-to-head signal that leads to $[Ca^{2+}]_i$ increase in the head, we

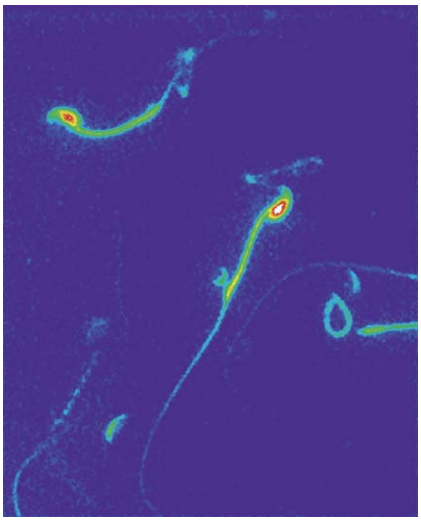

FIG. 2. Still from the Supplemental movie. A movie (QuickTime Video) showing the propagation of the increases in $[Ca^{2+}]$ along sperm flagella after application of 2 mM 8-Br-cGMP. Images are presented in a pseudocolor format (processed with NIH Image). Blue and red represent the low and high fluorescence signal levels, respectively. For clarity, cells with little movement were shown in this movie. The speed is six frames per second. Each frame represents 0.5 sec of real time (i.e., the movie is three times faster than real time). Upon the application of 8-Br-cGMP, $[Ca^{2+}]$ increases started in the principal piece and reached the head a few seconds later. At ~8 sec, ionomycin was added to the bath, resulting in $[Ca^{2+}]$ increases starting simultaneously along the cells.

wondered if this process also contributed to sperm capacitation and the AR.

We used the CTC fluorescence assay to examine the capacitation status of WT and *CatSper1*-mutant sperm after incubation with capacitation buffer. Successfully capacitated sperm were identified by the "B" fluorescence pattern after CTC staining (see *Materials and Methods*) [19, 33]. In agreement with the results observed with sperm tyrosine phosphorylation patterns [17], there was no difference in the CTC-assessed capacitation between the mutant and the WT sperm (Fig. 5A).

We also used the CTC assay to test whether the AR involves the principal piece-localized CATSPER channels. Buffer incubation was used as a negative control, and Ca^{2+} ionophore A23187-induced AR was used as a positive control. As shown in Figure 5B, A23187 (10 μM) induced similar percentages of AR in the WT and mutant sperm, suggesting that the exocytosis mechanisms downstream of $[Ca^{2+}]_i$ changes in the AR do not involve the CATSPER channel. Because the $[Ca^{2+}]_i$ increases, induced by 8-Br-cGMP or K8.6, were largely abolished in the *CatSper1*-mutant ([17] and Figs. 1 and 3), we wondered if the induced AR would be affected. To our surprise, the ARs, induced by either K8.6 or 8-Br-cGMP in the mutant, were nearly identical to those in the WT (Fig. 5B).

The CTC AR assay is based on the fluorescence emitted by CTC bound with divalent ions such as Ca^{2+} [19]. It therefore was possible that our CTC assay results in the null sperm had been artificially affected by the lack of the $[Ca^{2+}]_i$ increases induced by 8-Br-cGMP or K8.6. To rule out this possibility, we used the Coomassie blue staining method, which is based on cellular protein, to assay the AR rates. Again, no difference between the mutant and the WT was detected (Fig. 5C). We thus conclude that CATSPER1 is required for the increases in $[Ca^{2+}]_i$ but not for the AR.

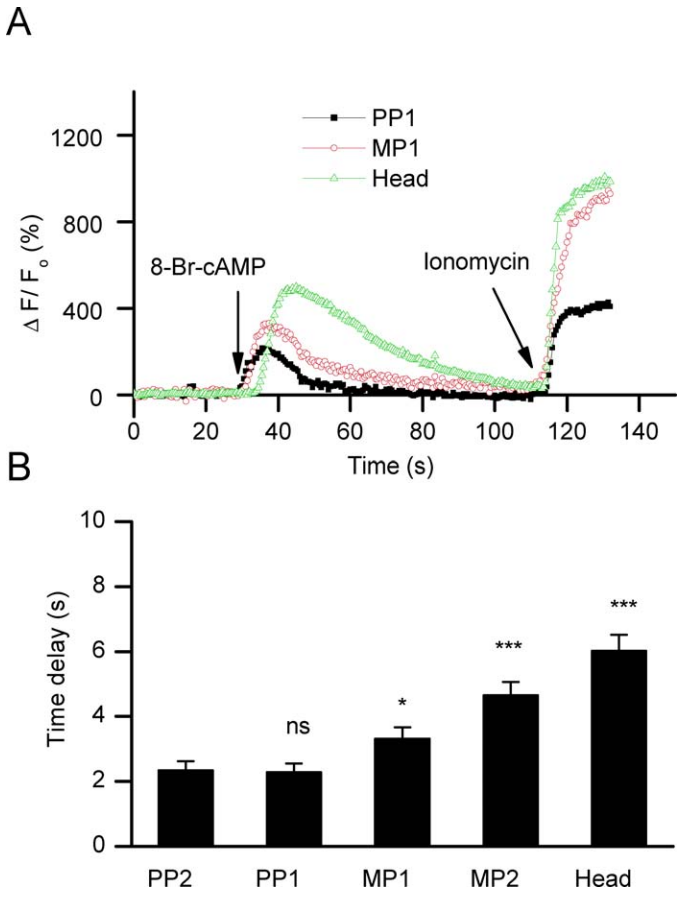

FIG. 3. A tail-to-head Ca^{2+} propagation induced by 8-Br-cAMP. **A**) Representative time courses of the $[Ca^{2+}]_i$ change in the principal piece (PP1), midpiece (MP1), and head from a WT sperm. **B**) Averaged time delays between the application of 8-Br-cAMP and the onset of the fluorescence change in the indicated subregions (n = 17, from two WT mice). See Figure 1 for a definition of the subregions.

Increases in [NADH] by the CATSPER-Dependent Ca^{2+} Influx

CATSPERs are required for the hyperactivated motility and may also be important for the maintenance of basal motility in mouse sperm [8, 11, 13, 14, 34]. In bull sperm, hyperactivation is triggered and maintained by Ca^{2+} [35]. Prolonged sperm hyperactivation presumably consumes extra ATP, which can be produced through oxidative phosphorylation in the midpiece mitochondria, or through glycolysis [36, 37]. In somatic cells, intracellular Ca^{2+} regulates NADH levels through the Ca^{2+}-sensitive dehydrogenases [38]. We imaged single-sperm NADH levels through its autofluorescence when excited at 360 nm [39]. Sodium cyanide (CN, an inhibitor of the mitochondrial respiratory chain complex IV) was used as a positive control for NADH imaging, because its application leads to a robust accumulation of NADH. Along the whole sperm, the midpiece showed the highest level of NADH autofluorescence, perhaps because of its high mitochondrial density. Weaker fluorescence was also observed in other regions of the cells, which likely reflected the cytosolic portion of NAD(P)H. Application of 8-Br-cGMP to the bath induced a robust, long-lasting increase in the NADH fluorescence level in the midpiece (Fig. 6A). The increase was largely abolished in the *CatSper1*-mutant sperm (Fig. 6B). The 8-Br-cGMP-induced NADH increase appeared to be specific for sperm;

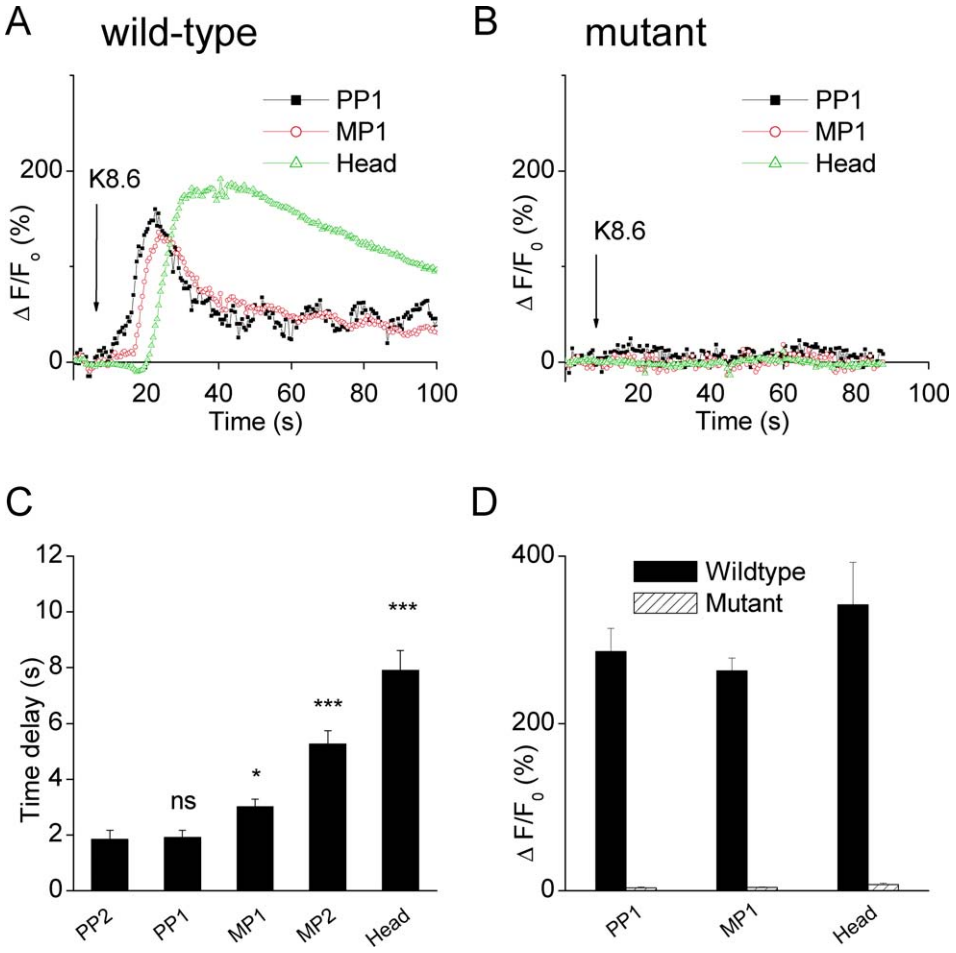

FIG. 4. A tail-to-head Ca^{2+} propagation induced by alkaline depolarization (K8.6). **A, B**) Representative time courses in a WT (**A**) and *CatSper*-null (**B**) sperm. **C**) Averaged time differences between the application of K8.6 and the onset of increases in the $\Delta F:F_0$ in subregions of WT sperm are shown (n = 10). (**D**) Averaged peak responses (n = 11 for WT and 15 for mutant).

similar treatment did not lead to detectable increases in HEK293 fibroblast cells (Fig. 6D). Furthermore, the NADH increase in sperm was not detectable when recorded in a Ca^{2+}-free bath (with 5 mM EGTA), implicating a role of Ca^{2+} entry (Fig. 6C). Taken together, these observations suggest that the 8-Br-cGMP-induced, CATSPER-dependent tail-to-head Ca^{2+} signaling induced an [NADH] increase in the midpiece.

Reduced ATP Level in CatSper1 *Mutant Sperm*

Because an increased in [NADH] may lead to ATP generation by the mitochondrial respiratory chain, we measured the ATP levels in the mutant and WT sperm. Compared with the WT, CATSPER1-deficient sperm had a reduced basal ATP level (Fig. 7A). Such a reduction was rescued in sperm from the transgenic mice expressing a GFP-CATSPER1 fusion protein in the mutant background (Tg in Fig. 7A). When challenged with 8-Br-cGMP, WT sperm had a slight increase in [ATP] (Fig. 7B). The mutant sperm, however, had a decrease. Again, the GFP-CATSPER1 protein in the transgenic sperm restored the [ATP] increase (Fig. 7B).

DISCUSSION

Our conclusion that the Ca^{2+} signal propagates from tail to head in the mouse sperm is based on two observations. First, there was a time delay (~3 sec) between the 8-Br-cGMP-induced $[Ca^{2+}]_i$ increases in the sperm head and principal piece. In contrast, no delay was detected when the increases in $[Ca^{2+}]_i$ were induced by ionomycin (Fig. 1). Second, the 8-Br-cGMP-induced increases in $[Ca^{2+}]_i$ were abolished in both the head and the tail in sperm lacking CATSPER1 protein, which is strictly localized along the principal piece. The simplest explanation of these data is that 8-Br-cGMP causes CATSPER channel opening (presumably through indirect mechanisms [12]); Ca^{2+} enters the principal piece; and the resulting Ca^{2+} triggers a tail-to-head propagation.

A tail-to-head Ca^{2+} propagation has also been reported in sea urchin sperm stimulated with the egg peptide speract, whose receptor activation presumably leads to the opening of an unidentified channel(s) in the tail [31]. Two CATSPER homologs have been cloned from sea urchin testis (Ren et al., unpublished results), but it remains to be determined if they, like the mouse homologs, are also localized in sperm flagella. In the sea urchin, the speract receptors were found in the sperm tails [40]. Similarly, olfactory receptors, along with the associated G protein (G_{olf}) and adenyl cyclases that may play roles in chemotaxis in some mammalian species, were also found in mammalian sperm tails [41, 42]. In human sperm, application of odorant bourgeonal initiates $[Ca^{2+}]_i$ increases and sperm chemotaxis. The increases in $[Ca^{2+}]_i$ were reported to start in the midpiece first and in the head a few seconds later [42]. Despite the apparent differences between the initiation sites of the Ca^{2+} signals induced by 8-Br-cGMP in the mouse and by odorant ligand in human sperm, it would be interesting to examine if both of them involve the activation of CATSPER channels, which are well conserved between humans and mice [8, 10, 11, 13].

The mechanisms by which cyclic nucleotides lead to the CATSPER-dependent $[Ca^{2+}]_i$ increase are not clear. Patch clamp recording apparently suggests that cyclic nucleotides do not directly open CATSPER channels [12], consistent with a

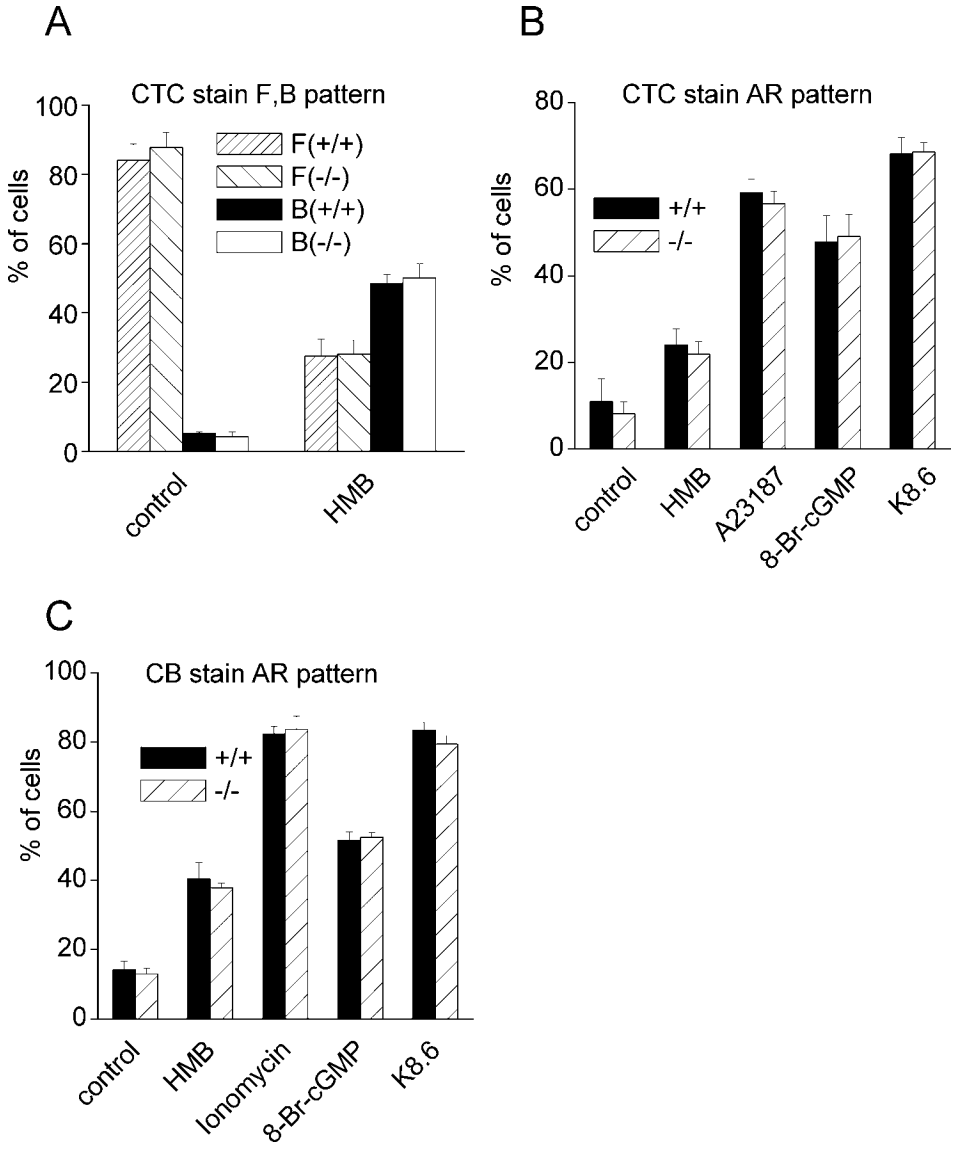

FIG. 5. CATSPER1 is not required for capacitation or the AR. Sperm from *CatSper1* mutant (−/−) and WT (+/+) were capacitated and treated with buffer (HMB), A23187 (10 μM), ionomycin (5 μM), 8-Br-cGMP (2 mM), or K8.6. Patterns in **A** and **B** were distinguished by the CTC assay and assigned as "F" (noncapacitated), "B" (successfully capacitated but not acrosome reacted), or "AR" (acrosome reacted). "Control" indicates samples withdrawn immediately before stimulus application. The AR rate assays were also repeated with the Coomassie blue staining (CB) method (**C**). N > 300 (from at least three pairs of mutant/WT mice).

lack of putative cyclic nucleotide binding domains in the CatSper channel proteins [8]. Furthermore, we used high concentrations of 8-Br-cGMP (2 mM) and 8-Br-cAMP (1 mM) to maximize the signals for a robust detection of the $[Ca^{2+}]_i$ propagation. Future studies are needed to examine the more physiologically relevant stimuli, such as bicarbonate and progesterone.

How does a Ca^{2+} entry through CATSPER channels in the principal piece trigger the $[Ca^{2+}]$ increase >10 μm away, in the sperm head? Our data show that there is a wavelike propagation through the midpiece. Hypothetically, Ca^{2+} entering through CATSPER channels can directly diffuse to the sperm head and lead to a $[Ca^{2+}]$ increase. This simple diffusion mechanism, however, is less likely. First, the distance between the head and the principal piece seems to be too large for a meaningful buildup in the head by simple diffusion. In Xenopus oocytes, for example, the Ca^{2+} diffusion constant was estimated to be <100 μm^2/sec (depending on the Ca^{2+} concentration), and a free Ca^{2+} ion was estimated to travel only ~0.1 μm before being buffered [43]. The sperm cell geometry, which can be modeled as a narrow and long tube, makes a one-dimensional approach to Ca^{2+} diffusion reasonable. These differences may enable Ca^{2+} ions to diffuse longer distances along the sperm flagellum than in Xenopus oocytes. Second, the $[Ca^{2+}]$ increase in principal piece was more transient than that in the midpiece and head (Fig. 1A), making it unlikely that the significant part of the Ca^{2+} increase in head was directly from the Ca^{2+} entry through CATSPER channels. More likely, Ca^{2+} entering the principal piece is used as a signal to trigger either Ca^{2+} release from intracellular stores or Ca^{2+} entry through plasma membrane channels in the midpiece and head, similar to the Ca^{2+}-induced Ca^{2+} release observed in many other cells [44]. Several plasma membrane channels and intracellular Ca^{2+} stores have been detected in sperm flagella [5, 36]. The mechanism of the tail-to-head Ca^{2+} propagation and the sources of the Ca^{2+} are currently under investigation.

It is known that Ca^{2+} signaling triggers spatially segregated physiological responses, such as the AR in the head and motility in the tail, but the relationship between the responses and the sources of Ca^{2+} is less clear [45]. Because sperm without the CATSPER1 protein retain the apparently intact ability to undergo capacitation and the AR (Fig. 5), the *CatSper1*-null mouse genetically separates the Ca^{2+} sources required for the AR and the hyperactivated sperm motility. The $[Ca^{2+}]_i$ increase required for the zona pellucida-induced AR is proposed to be from the TRP and other channels [6, 46]. As

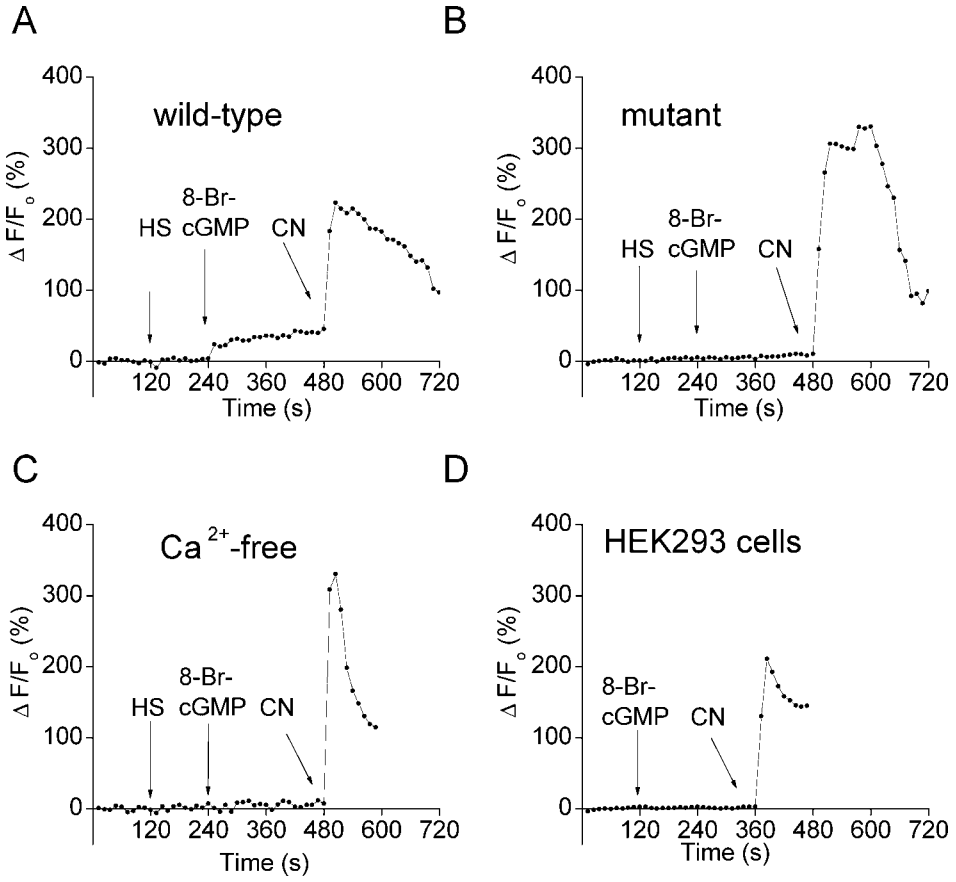

FIG. 6. [NADH] increases trigged by CATSPER-dependent Ca^{2+} propagation. NADH levels (as reflected by the averaged autofluorescence excited at 360 nm) were monitored when sperm were stimulated with buffer (HS), 8-Br-cGMP (2 mM), or sodium cyanide (CN, 1 mM) in the WT (**A**, n = 40) or the mutant (**B**, n = 47). No significant 8-Br-cGMP-induced NADH change was observed in WT sperm in the Ca^{2+}-free bath with 5 mM EGTA (**C**, n = 12). The 8-Br-cGMP did not induce NADH change in HEK293 fibroblast cells (**D**, n = 11).

reported by others [16, 47], we showed that cell-permeable cGMP induced AR (Fig. 5). Since 8-Br-cGMP triggers $[Ca^{2+}]_i$ increases in the head, we initially expected that the 8-Br-cGMP-induced AR was due to this increase in $[Ca^{2+}]_i$. In the *CatSper1*-mutant sperm, however, the 8-Br-cGMP-induced AR was not affected, even though the $[Ca^{2+}]_i$ increases were largely abolished in both the tail and head (Figs. 1 and 4). Sperm deficient in either CATSPER1 or CATSPER2 largely lack the depolarization (K8.6)-triggered $[Ca^{2+}]_i$ increases [14, 17]. With single-cell imaging, we extended these observations and found that K8.6, like 8-Br-cGMP, activated a tail-to-head Ca^{2+} propagation. Surprisingly, the mutant sperm retained the intact AR sensitivity to K8.6 (Fig. 5). Thus, we provided two cases (8-Br-cGMP and K8.6) in which the AR seems to be separated from the increases in $[Ca^{2+}]_i$ we observed in the head. One possible explanation would be that the 8-Br-cGMP-induced AR was caused by a $[Ca^{2+}]_i$ change independent of CATSPER1. If so, the increase in $[Ca^{2+}]_i$ that triggered the AR was likely small and below our detection limit. Alternatively, a CATSPER-independent $[Ca^{2+}]_i$ change contributing to the AR was highly transient, extremely slow, and/or strictly localized in "microdomains," which was beyond our temporal-spatial

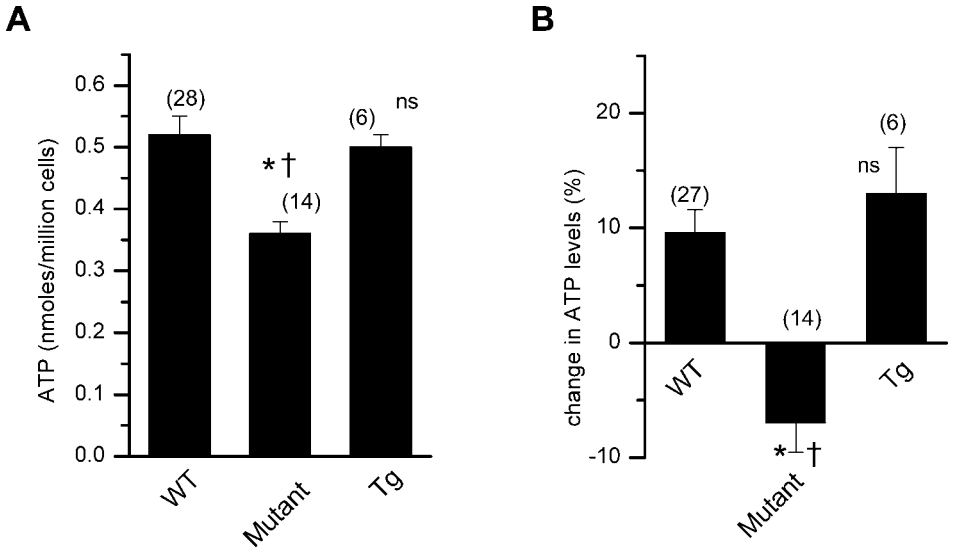

FIG. 7. Lower ATP level in CATSPER1-deficient sperm. **A**) Basal ATP levels in sperm from WT, *CatSper1*-null (mutant), and GFP-CATSPER1 transgene-rescued mutant (Tg). **B**) Averaged percent changes in ATP levels induced by 8-Br-cGMP application. Percent change for each preparation was calculated from the ATP levels in HS-treated and 8-Br-cGMP-treated samples. Numbers of measurements are in parentheses. Data were from eight WT, four mutant, and two transgenic mice. *, Statistically significant compared with WT ($P < 0.05$); NS, not statistically significant ($P > 0.05$); †, significant ($P < 0.05$) compared with Tg.

resolution. Furthermore, 8-Br-cGMP could "potentiate" the AR without a requirement for $[Ca^{2+}]_i$ increase.

The sperm midpiece displayed a ~40% increase of NADH autofluorescence when stimulated with 8-Br-cGMP (Fig. 6). In hepatocyte mitochondria stimulated with hormone [27], the NADH fluorescence increase was ~5%. A similar degree of increases was observed in neurons stimulated electrically [48]. How did the Ca^{2+} signal lead to the NADH increase? In somatic cells, the three Ca^{2+}-sensitive dehydrogenases (pyruvate dehydrogenase [PDH], NAD^+-isocitrate dehydrogenase [NAD-ICDH], and oxoglutarate dehydrogenase [OGDH]) are targets for the regulation of mitochondrial metabolism by Ca^{2+}, either through direct binding between Ca^{2+} and dehydrogenases (NAD-ICDH and OGDH) or through dehydrogenase phosphorylation in the case of PDH [38]. In the mouse sperm, mitochondria absorb Ca^{2+} and help maintain the low basal $[Ca^{2+}]_i$ [2]. Hypothetically, the cytosolic $[Ca^{2+}]$ increase and/or the absorbed Ca^{2+} may alter the NADH levels in the midpiece through Ca^{2+}-sensitive dehydrogenases. The mutant sperm have a lower ATP level, which may be related to the potentially lower basal $[Ca^{2+}]_i$ observed in the *CatSper*-mutant sperm [34]. The reduced basal ATP level may also explain the progressive loss of motility in the *CatSper*-mutant sperm [11]. Taken together, these data suggest that Ca^{2+} influx through the CATSPER channels is involved in ATP homeostasis. The molecular details of such a Ca^{2+} regulation remain to be further examined.

ACKNOWLEDGMENTS

We thank Dr. Bayard Storey for showing us the CTC and Coomassie staining methods, Drs. Donner Babcock, David Clapham, Betsy Navarro, and Lixia Yue for critically reading an earlier version of the manuscript, and Dr. Victor Vacquier for a sea urchin testis cDNA library.

REFERENCES

1. Yanagimachi R. Mammalian fertilization. In: Knobil E, Neill JD (eds.), The Physiology of Reproduction, 2nd ed. New York: Raven Press; 1994: 189–315.
2. Wennemuth G, Babcock DF, Hille B. Calcium clearance mechanisms of mouse sperm. J Gen Physiol 2003; 122:115–128.
3. Evans JP, Florman HM. The state of the union: the cell biology of fertilization. Nat Cell Biol Nat Med 2002:S57–S63.
4. Suarez SS, Ho HC. Hyperactivated motility in sperm. Reprod Domest Anim 2003; 38:119–124.
5. Darszon A, Nishigaki T, Wood C, Trevino CL, Felix R, Beltran C. Calcium channels and Ca^{2+} fluctuations in sperm physiology. Int Rev Cytol 2005; 243:79–172.
6. Jungnickel MK, Marrero H, Birnbaumer L, Lemos JR, Florman HM. Trp2 regulates entry of Ca^{2+} into mouse sperm triggered by egg ZP3. Nat Cell Biol 2001; 3:499–502.
7. Quill TA, Ren D, Clapham DE, Garbers DL. A voltage-gated ion channel expressed specifically in spermatozoa. Proc Natl Acad Sci U S A 2001; 98:12527–12531.
8. Ren D, Navarro B, Perez G, Jackson AC, Hsu S, Shi Q, Tilly JL, Clapham DE. A sperm ion channel required for sperm motility and male fertility. Nature 2001; 413:603–609.
9. Jin JL, O'Doherty AM, Wang S, Zheng H, Sanders KM, Yan W. Catsper3 and catsper4 encode two cation channel-like proteins exclusively expressed in the testis. Biol Reprod 2005; 73:1235–1242.
10. Lobley A, Pierron V, Reynolds L, Allen L, Michalovich D. Identification of human and mouse CatSper3 and CatSper4 genes: characterisation of a common interaction domain and evidence for expression in testis. Reprod Biol Endocrinol 2003; 1:53–67.
11. Qi H, Moran MM, Navarro B, Chong JA, Krapivinsky G, Krapivinsky L, Kirichok Y, Ramsey IS, Quill TA, Clapham DE. All four CatSper ion channel proteins are required for male fertility and sperm cell hyperactivated motility. Proc Natl Acad Sci U S A 2007; 104:1219–1223.
12. Kirichok Y, Navarro B, Clapham DE. Whole-cell patch clamp measurements of spermatozoa reveal an alkaline-activated Ca^{2+} channel. Nature 2006; 439:737–740.
13. Quill TA, Sugden SA, Rossi KL, Doolittle LK, Hammer RE, Garbers DL. Hyperactivated sperm motility driven by CatSper2 is required for fertilization. Proc Natl Acad Sci U S A 2003; 100:14869–14874.
14. Carlson AE, Quill TA, Westenbroek RE, Schuh SM, Hille B, Babcock DF. Identical phenotypes of CatSper1 and CatSper2 null sperm. J Biol Chem 2005; 280:32238–32244.
15. Wiesner B, Weiner J, Middendorff R, Hagen V, Kaupp UB, Weyand I. Cyclic nucleotide-gated channels on the flagellum control Ca2+ entry into sperm. J Cell Biol 1998; 142:473–484.
16. Kobori H, Miyazaki S, Kuwabara Y. Characterization of intracellular Ca^{2+} increase in response to progesterone and cyclic nucleotides in mouse spermatozoa. Biol Reprod 2000; 63:113–120.
17. Carlson AE, Westenbroek RE, Quill T, Ren D, Clapham DE, Hille B, Garbers DL, Babcock DF. CatSper1 required for evoked Ca^{2+} entry and control of flagellar function in sperm. Proc Natl Acad Sci U S A 2003; 100:14864–14868.
18. Wennemuth G, Westenbroek RE, Xu T, Hille B, Babcock DF. $Ca_V2.2$ and $Ca_V2.3$ (N- and R-type) Ca^{2+} channels in depolarization-evoked entry of Ca^{2+} into mouse sperm. J Biol Chem 2000; 275:21210–21217.
19. Saling PM, Storey BT. Mouse gamete interactions during fertilization in vitro. Chlortetracycline as a fluorescent probe for the mouse sperm acrosome reaction. J Cell Biol 1979; 83:544–555.
20. Adeoya-Osiguwa SA, Markoulaki S, Pocock V, Milligan SR, Fraser LR. 17beta-Estradiol and environmental estrogens significantly affect mammalian sperm function. Hum Reprod 2003; 18:100–107.
21. Pietrobon EO, Dominguez LA, Vincenti AE, Burgos MH, Fornes MW. Detection of the mouse acrosome reaction by acid phosphatase. Comparison with chlortetracycline and electron microscopy. J Androl 2001; 22:96–103.
22. Florman HM, Corron ME, Kim TD, Babcock DF. Activation of voltage-dependent calcium channels of mammalian sperm is required for zona pellucida-induced acrosomal exocytosis. Dev Biol 1992; 152:304–314.
23. Larson JL, Miller DJ. Simple histochemical stain for acrosomes on sperm from several species. Mol Reprod Dev 1999; 52:445–449.
24. Thaler CD, Cardullo RA. Biochemical characterization of a glycosylphosphatidylinositol-linked hyaluronidase on mouse sperm. Biochemistry 1995; 34:7788–7795.
25. Arnoult C, Cardullo RA, Lemos JR, Florman HM. Activation of mouse sperm T-type Ca^{2+} channels by adhesion to the egg zona pellucida. Proc Natl Acad Sci U S A 1996; 93:13004–13009.
26. Pralong WF, Hunyady L, Varnai P, Wollheim CB, Spat A. Pyridine nucleotide redox state parallels production of aldosterone in potassium-stimulated adrenal glomerulosa cells. Proc Natl Acad Sci U S A 1992; 89: 132–136.
27. Hajnoczky G, Robb-Gaspers LD, Seitz MB, Thomas AP. Decoding of cytosolic calcium oscillations in the mitochondria. Cell 1995; 82:415–424.
28. Dumollard R, Marangos P, Fitzharris G, Swann K, Duchen M, Carroll J. Sperm-triggered $[Ca^{2+}]$ oscillations and Ca^{2+} homeostasis in the mouse egg have an absolute requirement for mitochondrial ATP production. Development 2004; 131:3057–3067.
29. Miki K, Qu W, Goulding EH, Willis WD, Bunch DO, Strader LF, Perreault SD, Eddy EM, O'Brien DA. Glyceraldehyde 3-phosphate dehydrogenase-S, a sperm-specific glycolytic enzyme, is required for sperm motility and male fertility. Proc Natl Acad Sci U S A 2004; 101: 16501–16506.
30. Reigada D, Lu W, Mitchell CH. Glutamate acts at NMDA receptors on fresh bovine and on cultured human retinal pigment epithelial cells to trigger release of ATP. J Physiol 2006; 575:707–720.
31. Wood CD, Darszon A, Whitaker M. Speract induces calcium oscillations in the sperm tail. J Cell Biol 2003; 161:89–101.
32. Babcock DF, Pfeiffer DR. Independent elevation of cytosolic $[Ca^{2+}]$ and pH of mammalian sperm by voltage-dependent and pH-sensitive mechanisms. J Biol Chem 1987; 262:15041–15047.
33. Ward CR, Storey BT. Determination of the time course of capacitation in mouse spermatozoa using a chlortetracycline fluorescence assay. Dev Biol 1984; 104:287–296.
34. Marquez B, Ignotz G, Suarez SS. Contributions of extracellular and intracellular Ca^{2+} to regulation of sperm motility: release of intracellular stores can hyperactivate CatSper1 and CatSper2 null sperm. Dev Biol 2007; 303:214–221.
35. Ho HC, Granish KA, Suarez SS. Hyperactivated motility of bull sperm is triggered at the axoneme by Ca^{2+} and not cAMP. Dev Biol 2002; 250: 208–217.
36. Ho HC, Suarez SS. Characterization of the intracellular calcium store at the base of the sperm flagellum that regulates hyperactivated motility. Biol Reprod 2003; 68:1590–1596.
37. Travis AJ, Jorgez CJ, Merdiushev T, Jones BH, Dess DM, Diaz-Cueto L,

Storey BT, Kopf GS, Moss SB. Functional relationships between capacitation-dependent cell signaling and compartmentalized metabolic pathways in murine spermatozoa. J Biol Chem 2001; 276:7630–7636.
38. McCormack JG, Halestrap AP, Denton RM. Role of calcium ions in regulation of mammalian intramitochondrial metabolism. Physiol Rev 1990; 70:391–425.
39. Pralong WF, Spat A, Wollheim CB. Dynamic pacing of cell metabolism by intracellular Ca2+ transients. J Biol Chem 1994; 269:27310–27314.
40. Cardullo RA, Herrick SB, Peterson MJ, Dangott LJ. Speract receptors are localized on sea urchin sperm flagella using a fluorescent peptide analog. Dev Biol 1994; 162:600–607.
41. Vanderhaeghen P, Schurmans S, Vassart G, Parmentier M. Olfactory receptors are displayed on dog mature sperm cells. J Cell Biol 1993; 123: 1441–1452.
42. Spehr M, Schwane K, Riffell JA, Barbour J, Zimmer RK, Neuhaus EM, Hatt H. Particulate adenylate cyclase plays a key role in human sperm olfactory receptor-mediated chemotaxis. J Biol Chem 2004; 279:40194–40203.
43. Allbritton NL, Meyer T, Stryer L. Range of messenger action of calcium ion and inositol 1,4,5-trisphosphate. Science 1992; 258:1812–1815.
44. Berridge MJ, Bootman MD, Roderick HL. Calcium signalling: dynamics, homeostasis and remodelling. Nat Rev Mol Cell Biol 2003; 4:517–529.
45. Marquez B, Suarez SS. Different signaling pathways in bovine sperm regulate capacitation and hyperactivation. Biol Reprod 2004; 70:1626–1633.
46. O'Toole CM, Arnoult C, Darszon A, Steinhardt RA, Florman HM. Ca^{2+} entry through store-operated channels in mouse sperm is initiated by egg ZP3 and drives the acrosome reaction. Mol Biol Cell 2000; 11:1571–1584.
47. Santos-Sacchi J, Gordon M. Induction of the acrosome reaction in guinea pig spermatozoa by cGMP analogues. J Cell Biol 1980; 85:798–803.
48. Kasischke KA, Vishwasrao HD, Fisher PJ, Zipfel WR, Webb WW. Neural activity triggers neuronal oxidative metabolism followed by astrocytic glycolysis. Science 2004; 305:99–103.